



RESEARCH LETTER

10.1029/2018GL079023

How Asymmetries Between Arctic and Antarctic Climate Sensitivity Are Modified by the Ocean

H. A. Singh^{1,2}, O. A. Garuba¹, and P. J. Rasch¹

¹Atmospheric Sciences and Global Change Division, Pacific Northwest National Laboratory, U.S. Department of Energy Office of Science, Richland, WA, USA, ²School of Earth and Ocean Sciences, University of Victoria, Victoria, British Columbia, Canada

Key Points:

- The Arctic has greater intrinsic sensitivity to ocean state changes than the Antarctic
- The ocean response triggers more destabilizing radiative feedbacks over the Arctic than the Antarctic
- Polar radiative feedbacks respond more to increased high-latitude ocean heat convergence than to subpolar ocean heat uptake

Supporting Information:

- Supporting Information S1

Correspondence to:

H. A. Singh, hansis.singh@pnnl.gov

Citation:

Singh, H. A., Garuba, O. A., & Rasch, P. J. (2018). How asymmetries between Arctic and Antarctic climate sensitivity are modified by the ocean. *Geophysical Research Letters*, 45, 13,031–13,040. <https://doi.org/10.1029/2018GL079023>

Received 5 JUN 2018

Accepted 31 OCT 2018

Accepted article online 5 NOV 2018

Published online 12 DEC 2018

Abstract We investigate how the ocean response to CO₂ forcing affects hemispheric asymmetries in polar climate sensitivity. Intermodel comparison of Phase 5 of the Coupled Model Intercomparison Project CO₂ quadrupling experiments shows that even in models where hemispheric ocean heat uptake differences are small, Arctic warming still exceeds Antarctic warming. The polar climate impact of this evolving ocean response to CO₂ forcing is then isolated using slab ocean experiments in a state-of-the-art climate model. Overall, feedbacks over the Southern Hemisphere more effectively dissipate top-of-atmosphere anomalies than those over the Northern Hemisphere. Furthermore, a poleward shift in ocean heat convergence in both hemispheres amplifies destabilizing ice albedo and lapse rate feedbacks over the Arctic much more so than over the Antarctic. These results suggest that the Arctic is intrinsically more sensitive to both CO₂ and oceanic forcings than the Antarctic and that ocean-driven climate sensitivity asymmetry arises from feedback destabilization over the Arctic rather than feedback stabilization over the Antarctic.

Plain Language Summary Anthropogenic greenhouse gas emissions impact climate globally, but nowhere more so than over the Arctic, a phenomenon known as *polar amplification*. Surprisingly, the climate response over the Antarctic is much more muted than the climate response over the Arctic, which has been attributed to the large uptake of heat over the Southern Ocean which cools the Southern Hemisphere. Here we show that a weaker climate response over the Antarctic is due, in part, to weaker intrinsic sensitivity to both greenhouse gas forcing and the state of the ocean. Even climate models with similar amounts of heat uptake into the deep ocean in both hemispheres warm more over the Arctic than the Antarctic. Furthermore, similar increases in winter season heat transport into the polar oceans in both hemispheres trigger more destabilizing climate feedbacks over the Arctic than the Antarctic. Therefore, greater climate change over the Arctic than the Antarctic can be expected even if ocean heat uptake or ocean heat transport changes are similar in both hemispheres.

1. Introduction

Asymmetry of the climate change signal in the Arctic and the Antarctic is evident in current observations and modeling studies (Turner et al., 2007; Walsh, 2009). While sea ice extent has been trending downward in the Arctic (Comiso, 2002; Stroeve et al., 2007), it has been modestly increasing in the Antarctic (Fetterer et al., 2017; Turner et al., 2009; though observations over the past 2 years have shown a sharp decline in Antarctic sea ice extent). Winter season temperatures have been trending upward over most of the Arctic (Comiso, 2003), but the Antarctic has shown more mixed trends, with cooling over the East Antarctic accompanied by warming over the West Antarctic and its peninsula (Steig et al., 2009). Global climate models (GCMs) project receding sea ice in both hemispheres, but ice loss and warming over the Antarctic are still more muted than that over the Arctic in nearly all models (Knutti & Sedlacek, 2013).

Several hypotheses have been put forth to explain the asymmetric climate response over the Earth's polar regions. Diminished stratospheric ozone (and its associated circulation changes; see, e.g., Turner et al., 2009), greater freshwater fluxes from Antarctic ice shelf melt (Bintanja et al., 2013), and greater sequestration of heat in the deep Southern Ocean (Flato & Boer, 2001) have all been proposed to decrease transient climate sensitivity over the Antarctic. The mean state Southern Ocean circulation has also been proposed to delay Antarctic warming, as northward Ekman transport advects greenhouse-warmed waters away from the continent, which are replaced by cooler upwelled waters from the deep (Armour et al., 2016; Marshall et al., 2014).

©2018. American Geophysical Union. All Rights Reserved.

This is an open access article under the terms of the Creative Commons Attribution-NonCommercial-NoDerivs License, which permits use and distribution in any medium, provided the original work is properly cited, the use is non-commercial and no modifications or adaptations are made.

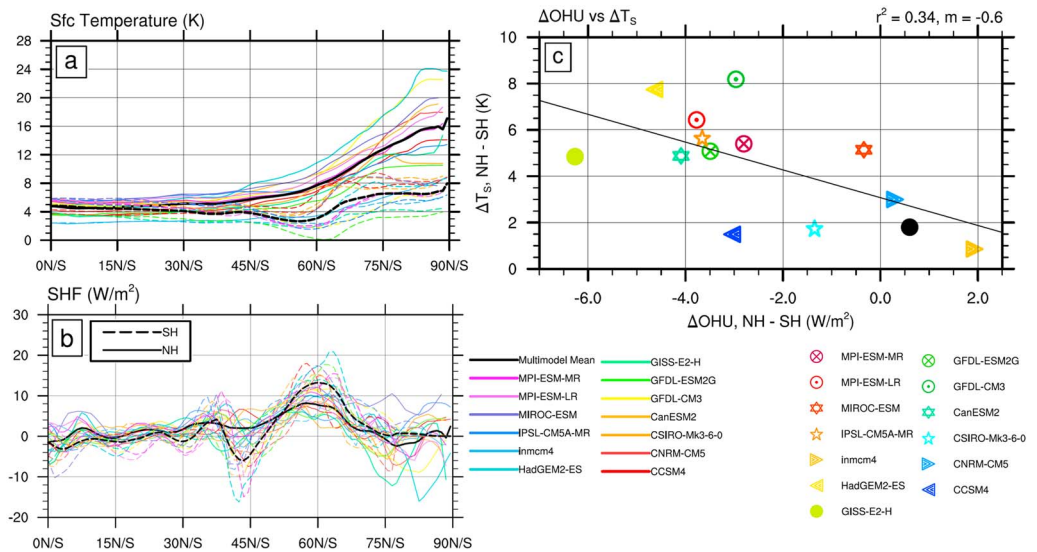


Figure 1. Response to CO₂ quadrupling (years 100–150) in 13 CMIP5 models: (a) zonal mean surface temperature anomaly (K) in the Northern Hemisphere (NH; solid lines) and Southern Hemisphere (SH; dashed lines) in individual CMIP5 models (colors) and for the multimodel mean (black). (b) As in (a) but for the ocean heat uptake (OHU) anomaly (W/m²; positive downward). (c) OHU difference between the NH and SH (area weighted and averaged from 50°N/S to the pole) versus the area-averaged polar temperature anomaly difference between the NH and SH (area weighted and averaged from 50°N/S to the pole), for individual CMIP5 models (markers) with the line of best fit computed via linear regression (y intercept = 3.2 K, slope = 0.6 K/W/m², $r = 0.6$). In (c), results from years 300 to 330 of the CESM1 CO₂ doubling experiment are also shown (black dot).

Taken together, these hypotheses all ascribe a prominent role for the ocean in decreasing transient sensitivity over the Antarctic, through its response to changing momentum, freshwater, or heat fluxes (though the impacts of ozone depletion and ice shelf melt in opposing warming have both been contested; see, e.g., Pauling et al., 2016; Sigmund & Fyfe, 2010). Conversely, high sensitivity over the Arctic has largely been attributed to stronger local feedback processes (Hwang et al., 2011; Kay et al., 2012), with increased ocean heat transport also augmenting sensitivity (Holland & Bitz, 2003; Hwang & Frierson, 2010).

Despite these differing narratives, there are similarities between the ocean heat transport and uptake responses in both hemispheres. Some models show an increase in ocean heat transport in winter in both the Arctic and Antarctic (Singh et al., 2017). Others have substantial ocean heat uptake (OHU) in the subpolar North Atlantic which rivals uptake over the Southern Ocean (see Rose & Rayborn, 2016, Figure 1). How sensitive are polar climates to these ocean responses, namely, increased ocean heat transport combined with evolving subpolar heat uptake? And to what extent can these ocean responses, and the radiative feedback responses to them, be used to explain differences in polar climate sensitivity between the Arctic and the Antarctic?

In this study, we examine whether differences in CO₂-forced OHU and convergence between the NH and SH, or different sensitivities to these ocean responses, may play a role in asymmetric climate sensitivities over the Arctic and Antarctic. We begin by examining polar warming asymmetries and their relationship to subpolar OHU in a collection of models participating in Phase 5 of the Coupled Model Intercomparison Project (CMIP5). We then directly impose evolving OHU and ocean heat transport changes (computed from a fully coupled CO₂ doubling experiment) in a climate model with a slab ocean and analyze the forcing efficacy and associated seasonal radiative feedbacks of this ocean response in both hemispheres. We use these results to assess the ocean's role in enhancing Arctic-Antarctic sensitivity asymmetries.

2. Methods

2.1. CMIP5 Analysis

The relationship between hemispheric surface temperature and OHU responses to CO₂ quadrupling is assessed in 13 models participating in CMIP5 (averaged poleward of 50°N/S for Figure 1c). Individual models used in the analysis are listed in the supporting information (SI) Table S1. We hereafter refer to the OHU as the

Table 1
Overview of CESM-SOM Experiments

Experiment	Atmosphere	Ocean	Net OHU (NH/SH)
Control	1XCO ₂	Control OHFC	0.0 W/m ²
PertAtm	2XCO ₂	Control OHFC	0.0 W/m ²
PertAtm+Ocn15	2XCO ₂	Pert OHFC, years 0–30	1.9 W/m ² (2.0/1.8)
PertAtm+Ocn85	2XCO ₂	Pert OHFC, years 60–90	1.2 W/m ² (1.3/1.1)
PertAtm+Ocn165	2XCO ₂	Pert OHFC, years 150–180	0.6 W/m ² (0.7/0.5)
PertAtm+Ocn485	2XCO ₂	Pert OHFC, years 470–500	0.1 W/m ² (0.2/0.0)

Note. The northern/southern hemispheric (NH/SH) OHU anomaly is quantified as the area-weighted integral of the net (downward) surface heat flux in the respective hemisphere. CESM = Community Earth System Model version 1; SOM = slab ocean model; OHU = ocean heat uptake; OHFC = ocean heat flux convergence.

net (positive downward) surface heat flux anomaly, which includes both radiative and turbulent components. For each model, anomalies are computed as the difference between a simulation where CO₂ was abruptly quadrupled (Ab4XCO₂, averaged over years 100–150) and a control simulation using preindustrial forcing (PIControl). To assess how hemispheric differences between the subpolar/polar surface temperature response are related to hemispheric differences in subpolar/polar OHU (Figure 1c), surface temperature anomalies and OHU are area weighted and averaged poleward of 50°N/S; the linear regression shown is relatively insensitive to the choice of this latitudinal cutoff (i.e., latitudes between 40°N/S and 60°N/S and the pole all yield similar relationships between hemispheric OHU differences and hemispheric surface temperature differences).

2.2. Experiments With the Fully Coupled CESM1

To assess the time-evolving ocean response to CO₂ doubling, a 500-year abrupt CO₂ doubling experiment is performed using the fully coupled Community Earth System Model version 1 (CESM1; Hurrell et al., 2013) with the following components, all at nominally 1° spatial resolution: the Community Atmosphere Model version 5 (CAM5; Neale et al., 2012), Parallel Ocean Program version 2 (Danabasoglu et al., 2012), the Los Alamos Sea Ice Model (Hunke & Lipscomb, 2008), and the Community Land Model version 4 (Oleson et al., 2010). Branching from an equilibrated preindustrial control run, atmospheric CO₂ is abruptly doubled from 284 to 568 ppm, with all other constituents held at preindustrial levels.

2.3. Experiments With the CESM Coupled to a Slab Ocean (CESM-SOM)

The time-evolving mixed layer ocean response to CO₂ doubling in the fully coupled CESM1 (over years 0–30, 60–90, 150–180, and 470–500) is captured using the *Q-flux* formulation of Bitz et al. (2012)

$$\rho_w c_p h_{ML} \frac{dT_{ML}}{dt} = F_{net} - Q_{fix}, \quad (1)$$

where ρ_w is the density of seawater, c_p is its heat capacity, h_{ML} is the annual mean depth of the mixed layer (see Bailey et al., 2010), F_{net} is the net surface heat flux, and Q_{fix} is the ocean heat flux convergence (hereafter OHFC). This OHFC captures time-varying anomalies in ocean heat transport with CO₂ doubling as well as OHU below the mixed layer; the latter is captured as an anomalous divergence of the ocean heat flux from the mixed layer (i.e., as a negative OHFC anomaly).

We then evaluate the climatic impact of the time-varying ocean state by imposing each of these distinct perturbed OHFC patterns (Pert OHFC; computed from the monthly mean of the fully coupled CO₂ doubling experiment over years 0–30, 60–90, 150–180, and 470–500, using equation (1)) in a version of the CESM1 where Parallel Ocean Program version 2 has been replaced by a slab ocean model (hereafter CESM-SOM; see Bitz et al., 2012; Hansen et al., 1984, for earlier implementations of the SOM). The climatic impact of each of the four ocean states is assessed by differencing the relevant PertAtm+OcnX CESM-SOM experiment (2XCO₂ with Pert OHFC derived from years X-15 to X+15 from the fully coupled CO₂ doubling experiment) from PertAtm (2XCO₂ with Control OHFC, which is computed from a fully coupled preindustrial control run). The climatic impact of CO₂ doubling, without any accompanying changes in the ocean state, is assessed as the difference between PertAtm and Control (1XCO₂ with Control OHFC). Each CESM-SOM experiment (listed in Table 1) is run for 60 years; climatologies are computed over the final 30 years, when the run can be considered to be in equilibrium.

2.4. Sensitivity and Radiative Feedback Analysis

The effective climate feedback parameter, λ_{eff} , is computed as

$$\lambda_{\text{eff}} = \frac{F - H - \nabla \cdot [\text{TET}]}{\Delta T}, \quad (2)$$

where F is the forcing (equal to 3.8 W/m^2 for CO_2 doubling in CAM5; see Gettelman et al., 2012), H is the hemispheric OHU (see Table 1), $\nabla \cdot [\text{TET}]$ is the hemispheric divergence of the total energy transport in the equilibrated CESM-SOM experiment (computed as the cross-equatorial energy transport anomaly per unit area over each hemisphere), and ΔT is the surface temperature change in the equilibrated CESM-SOM experiment. The efficacy of the OHU forcing is the ratio $\varepsilon = \lambda_{\text{eff}}^{2\text{XCO}_2} / \lambda_{\text{eff}}^{\text{OHU}}$, where $\lambda_{\text{eff}}^{2\text{XCO}_2}$ is computed from the PertAtm experiment. Because H is very close to zero for the experiment utilizing OHFC from years 470 to 500, neither $\lambda_{\text{eff}}^{\text{OHU}}$ nor ε are computed for this forcing.

Individual components of the global radiative feedback over the polar regions (water vapor longwave, water vapor shortwave, lapse rate, Planck, surface albedo, and cloud feedback components) are evaluated using the radiative kernel methodology (Soden et al., 2008), where the radiative feedback $\lambda_X \equiv \partial R_X / \partial T$ due to X at location ϕ is

$$\lambda_X(\phi) = \left. \frac{\partial R}{\partial X} \right|_{\phi} \frac{\Delta X(\phi)}{\Delta T}, \quad (3)$$

where $\left. \frac{\partial R}{\partial X} \right|_{\phi}$ is the radiative kernel for X (computed from CAM3; see Shell et al., 2008), $\Delta X(\phi)$ is the local change in X , and ΔT is the global surface temperature change. We use the radiative kernels described in Shell et al. (2008); radiative feedback parameter estimates have been shown to be relatively insensitive to the choice of feedback kernel (Soden et al., 2008). High-latitude feedbacks are computed for each hemisphere as the area-weighted integral of λ_X from 60°N/S to the pole.

3. Results

3.1. CMIP5 Intermodel Comparisons

One hundred years following abrupt CO_2 quadrupling, all CMIP5 models exhibit less warming over the Antarctic (Figure 1a) than the Arctic, with differences between the hemispheres exceeding 4 K (8 K) poleward of 60°N/S (75°N/S). On the other hand, while polar climate sensitivity is substantially greater over the Arctic than the Antarctic in all models (also see SI Figure S1), SH subpolar OHU does not exceed NH subpolar OHU in all models (Figures 1b and S2). Indeed, out of the 13 models compared in this study, two have greater net OHU in the NH than the SH 100 years following CO_2 quadrupling (see SI Figure S2c).

To assess the relationship between greater OHU in the SH (relative to the NH) and weaker polar climate sensitivity over the Antarctic (relative to the Arctic), we plot the interhemispheric OHU difference (poleward of 50°N/S) and the interhemispheric difference in warming over this same region (Figure 1c). If stronger hemispheric subpolar OHU was linked to weaker hemispheric warming with CO_2 forcing (and vice versa), we would expect that models with greater SH subpolar OHU than NH subpolar OHU would warm far less over the Antarctic than the Arctic compared to those models with more similar NH and SH subpolar OHU. Indeed, we find that models with more asymmetry in hemispheric OHU also have greater interhemispheric asymmetry in polar warming ($r = 0.6$). Overall, 0.6 K greater polar climate warming is expected per 1 W/m^2 of reduced OHU (relative to the other hemisphere; slope of best fit line in Figure 1c). However, even if OHU is identical in both the hemispheres, Arctic warming is expected to exceed Antarctic warming by $\sim 3 \text{ K}$ (y intercept in Figure 1c).

Though CMIP5 results suggest that greater hemispheric OHU is linked to weaker polar warming in that hemisphere, it is unclear whether this relationship is a causal one. Weaker hemispheric warming either may facilitate greater OHU (by prompting greater energy flux convergence; see, e.g., Hwang et al., 2011) or may be caused by it. Furthermore, these causal relationships may differ in the NH and SH; indeed, OHU over the Southern Ocean has been shown to be passive (i.e., atmosphere driven; see Armour et al., 2016; Garuba et al., 2017), while OHU over the North Atlantic depends on redistributive changes in the ocean circulation (i.e., active; see Garuba et al., 2017). Therefore, in order to assess the impact of OHU on the rest of the climate system, particularly the polar regions, we isolate this ocean response in a single model, impose it in a slab ocean framework, and analyze its high-latitude climatic impact.

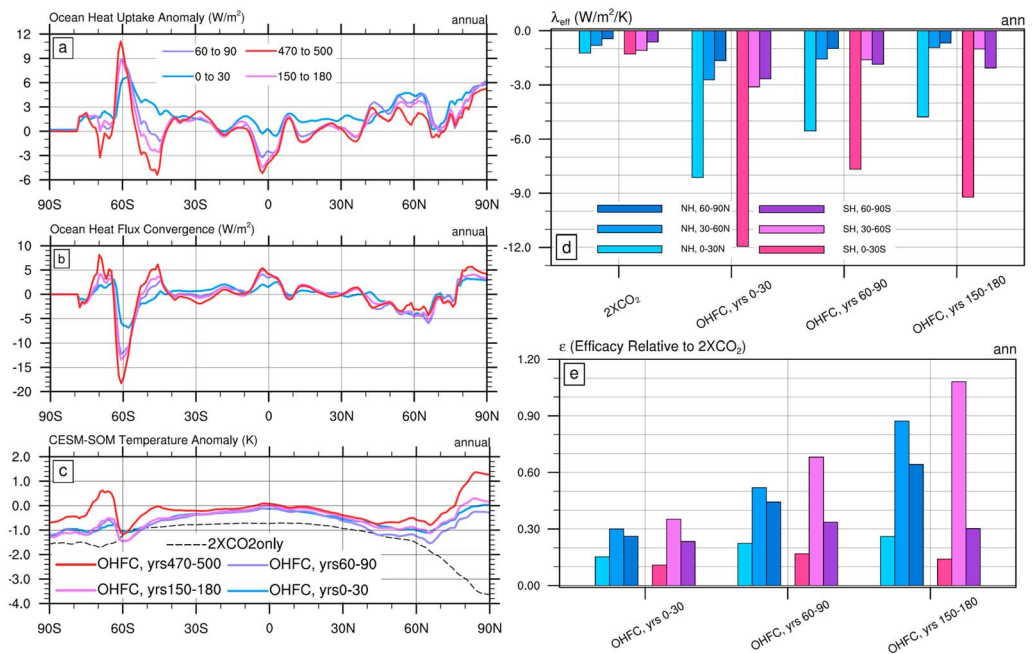


Figure 2. Ocean response to CO₂ doubling in the fully coupled CESM1 and impact of this ocean response in the CESM-SOM: (a) zonally averaged OHU (W/m²; positive downward) following CO₂ doubling in the fully coupled CESM1 over years 0–30, 60–90, 150–180, and 470–500. (b) As in (a) but for the ocean heat flux convergence (OHFC, W/m²) anomaly in the mixed layer. (c) Zonally averaged surface temperature impact (K) of the evolving OHFC anomaly (derived from the fully coupled CESM1, over years 0–30, 60–90, 150–180, and 470–500 following CO₂ doubling) in the CESM-SOM, computed as $\text{PertAtm} + \text{PertOcnX} - \text{PertAtm}$. (d) The effective feedback parameter (λ_{eff} , W/m²/K) for the 2XCO₂ and OHFC forcings, computed in each hemisphere for the tropics (0 to 30°N/S), midlatitudes (30°N/S to 60°N/S) and high latitudes (60°N/S to the pole). (e) The efficacy ϵ of the OHFC forcings relative to CO₂ doubling. In (c), the scaled (multiplied by $-1/4$) surface temperature response to CO₂ doubling in the CESM-SOM is also shown (dashed black line) and in (d) and (e), λ_{eff} and ϵ are not computed for the OHFC, years 470–500 SOM experiment since the hemispheric OHU is very small in this case (< 0.2 W/m²).

3.2. Ocean Response to CO₂ doubling and Its Climatic Impact

In the CESM1, CO₂ doubling warms the Arctic by 3 K more than it warms the Antarctic (see SI Figure S3) while OHU in the NH exceeds OHU in the SH by at least 0.2 W/m² (Figure S4; shown as black dot in Figure 1c for surface temperatures and OHU averaged poleward of 50°N/S). Following abrupt CO₂ doubling, the spatial pattern of the OHU evolves with time, from one that includes both tropical and subpolar heat uptake (years 0–30 in Figure 2a) to one where the largest heat uptake anomalies in each hemisphere are over the subpolar oceans (years 60–90, 150–180, and 470–500 in Figure 2a). The OHFC computed from these different time periods reflects these anomalies in the OHU (Figure 2b): subpolar OHU manifests as a negative OHFC anomaly $\sim 60^\circ$ N/S which equilibrates with time (i.e., the area-weighted average between subtropics and high latitudes becomes small). Increased OHFC into the polar oceans is also evident (at 80°N and 70°S; Figure 2b) and results from greater ocean heat transport into the high latitudes (which characterizes many GCMs with greater polar amplification; see, e.g., Holland & Bitz, 2003; Hwang et al., 2011).

As expected, imposing these OHFC anomalies as a forcing in the CESM-SOM (see section 2) induces global cooling (Figure 2c) because the net global OHU is negative. In both hemispheres, the regions of greatest cooling are $\sim 60^\circ$ N/S and are well collocated with regions of greatest OHU with CO₂ doubling in the fully coupled CESM (compare Figure 2c with Figure 2a). OHFC-induced cooling is minimal over the tropics and high latitudes; this signature contrasts sharply with the polar-amplified temperature response to CO₂ doubling (Figure 2c, black dashed line showing the scaled response with a change of sign).

The effective climate feedback parameter highlights regional and forcing-dependent differences in the climate response (Figure 2d). For a given forcing, feedbacks are most stabilizing (i.e., most effective at bringing the net top-of-atmosphere [TOA] anomaly closer to zero and, therefore, equilibrium) over the tropics and least stabilizing (i.e., least effective at bringing the net TOA anomaly closer to zero) over the high latitudes (except in the SH for the years 60–90 and 150–180 OHFC anomalies), which is consistent with greater climate

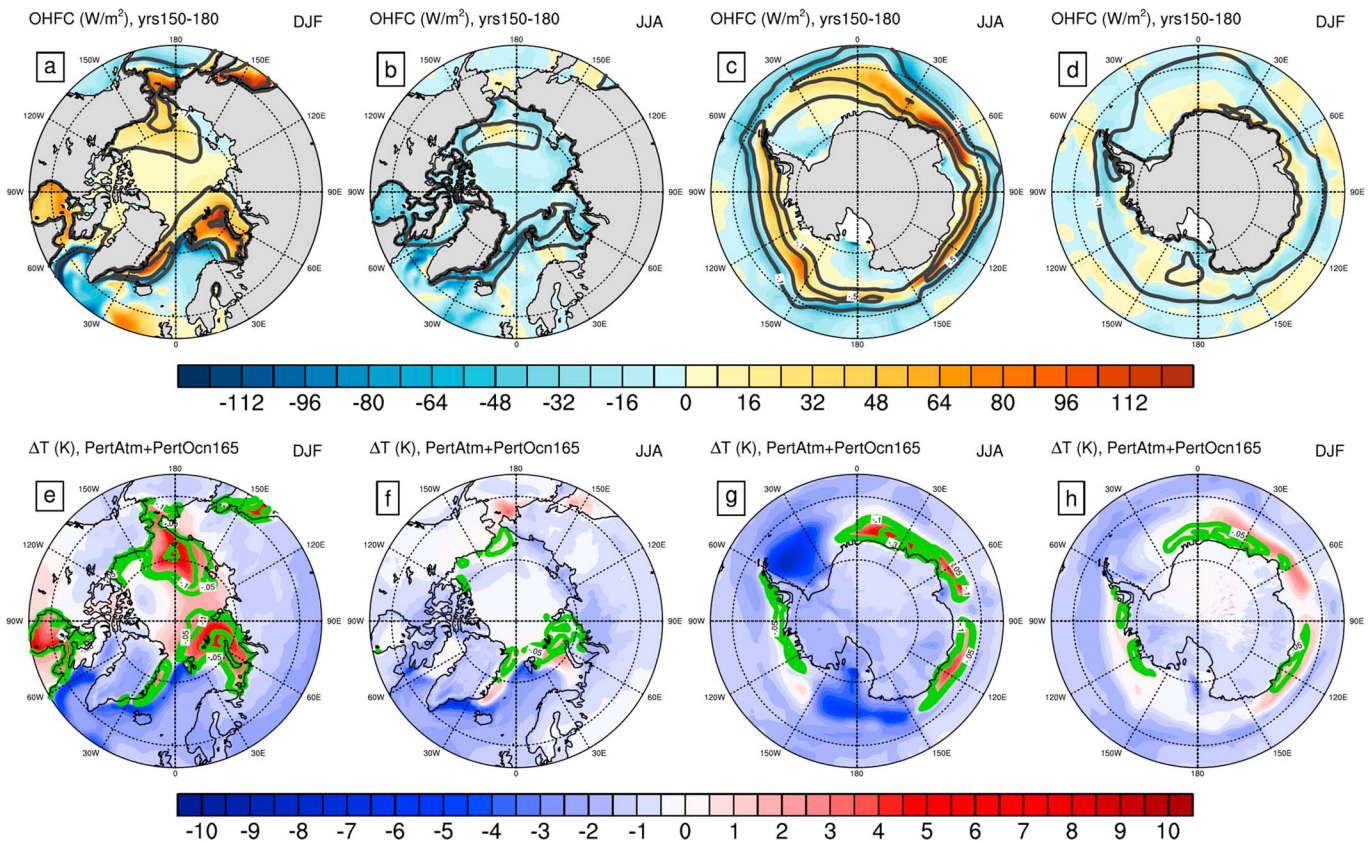


Figure 3. Seasonal ocean response to CO₂ doubling in the fully coupled CESM1 and seasonal impact of this ocean response in the CESM-SOM: (a–d) change in ocean heat flux convergence (OHFC; colors, W/m²) and sea ice fraction (contours) over years 150–180 following CO₂ doubling in the fully coupled CESM. (e–h) Seasonal change in temperature (colors, K) and sea ice fraction (contours) due to the years 150–180 OHFC change, calculated as PertAtm+PertOcn165 – PertAtm. Shown for the winter (a, c, e, and g; December-January-February [DJF] for the Arctic and June-July-August [JJA] for the Antarctic) and summer seasons (b, d, f, and h; JJA for the Arctic and DJF for the Antarctic) over the Arctic (a, b, e, and f) and Antarctic (c, d, g, and h).

sensitivity over the high latitudes (which results in polar amplification of the climate response; see, e.g., Manabe & Wetherald, 1975). The effective feedback is particularly stabilizing for the OHFC forcings in the tropics, since the tropics cool very little with the imposed OHFC (reflecting the tendency of extratropical forcings to elicit only muted responses over the tropics; see Alexeev et al., 2005). While cooling due to the anomalous OHFC appears roughly symmetric between the hemispheres (Figure 2c), the effective climate feedback parameter also highlights asymmetries between the NH and SH (Figure 2d). Over all regions (the tropics, 0–30°N/S; midlatitudes, 30°N/S to 60°N/S; and high latitudes, 60°N/S to 90°N/S), both CO₂ doubling and OHFC anomalies trigger less stabilizing feedbacks (i.e., less effective at pulling the net TOA anomaly back to zero) over the NH than the SH, suggesting intrinsic differences in sensitivity between the two hemispheres.

To assess the relative ability of the OHFC forcings to evoke temperature changes compared to CO₂ doubling, we examine the regional efficacy ϵ of each OHFC forcing (Figure 2e; assessed relative to the effective regional feedback due to CO₂ doubling; see section 2). OHFC forcings from years 0 to 30 and 60 to 90 have $\epsilon < 1$, indicating that CO₂ doubling evokes a greater temperature change per unit forcing than these oceanic forcings; on the other hand, the OHFC forcing from years 150 to 180 evokes similar temperature changes per unit forcing as CO₂ doubling alone, particularly over the midlatitudes ($\epsilon \approx 1$). Overall, the OHFC forcing efficacy is greatest over the midlatitudes in all experiments, where ϵ is greater over the SH than the NH; conversely, OHFC forcing efficacy is generally greater over the NH than the SH in the tropics and high latitudes. Compared to the midlatitudes, the efficacy of the OHFC forcing is surprisingly low over the high latitudes, even through the greatest OHFC forcings flank the polar oceans (~60°N/S; Figure 2b). This decreased forcing efficacy over the high latitudes can be understood in terms of the seasonal OHFC response to CO₂ doubling and the polar climate response to these OHFC anomalies, which we now explore further.

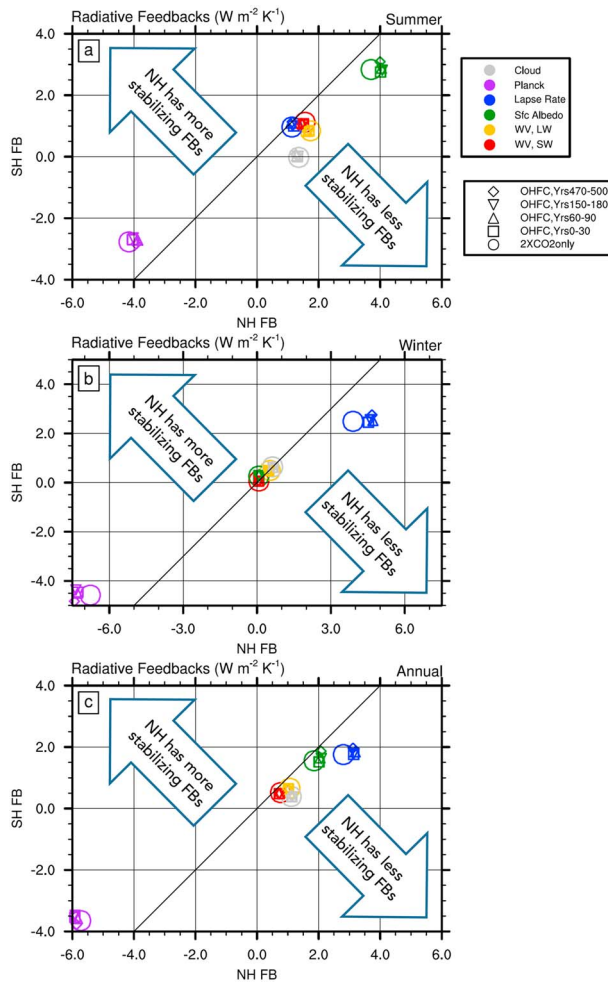


Figure 4. High-latitude feedback analysis of CESM-SOM experiments, comparing the Arctic and Antarctic: (a) winter season water vapor longwave (WV LW), water vapor shortwave (WV SW), cloud, lapse rate, Planck, and surface albedo feedbacks over the Arctic (60–90°N; December-January-February [DJF]) versus the Antarctic (60–90°S; June-July-August [JJA]) in PertAtm (2XCO₂ only; large circle markers) and PertAtm+OcnX (2XCO₂ with OHFC from years 0 to 30, 60 to 90, 150 to 180, and 470 to 500 of the fully coupled CO₂ doubling experiment; small markers) CESM-SOM experiments. (b) As in (a) but for the summer season (JJA for the Arctic and DJF for the Antarctic). (c) As in (a) but for the annual mean. The one-to-one line is also shown.

3.2.1. Seasonal OHFC Changes and Climate Responses Over the High Latitudes

With CO₂ doubling, OHFC anomalies are strongly seasonal over the high latitudes (Figures 3a–3d, shown over years 150–180 following CO₂ doubling). In winter, converging ocean heat at the sea ice edge contains ice extent in the preindustrial control climate (Bitz et al., 2005); when CO₂ is doubled, OHFC increases over polar latitudes and decreases over subpolar latitudes in both hemispheres in winter (Figures 3a and 3c), constituting a poleward OHFC shift that coincides with the retreating sea ice edge (see Bitz et al., 2006; Singh et al., 2017) and increases with time following CO₂ doubling in the fully coupled CESM (see SI Figure S5). This poleward OHFC shift reflects a winter season increase in ocean heat transport in the mixed layer in the high latitudes (Figure S6; 0.2-PW increase into the Arctic and 0.4-PW increase into the Antarctic in years 470–500 following CO₂ doubling) and corresponds closely to a poleward shift in winter season heat loss from the mixed layer (see SI Figure S7; also see Sutton & Mathieu, 2002, who show that OHFC anomalies are well collocated with upward turbulent heat flux anomalies). No similar poleward OHFC shift occurs in summer (Figures 3b and 3d).

The climatic impact of this highly seasonal OHFC forcing can be assessed in the CESM-SOM (by differencing the PertAtm+OcnX and PertAtm experiments). Increased ocean heating of the polar regions dominates the high-latitude climate response in winter, with increased surface temperatures and decreased sea ice (Figures 3e and 3g). The low efficacy of the OHFC forcings in the high latitudes (recall Figure 2e) is due to this ocean-driven warming of the polar regions in winter, which opposes the general global cooling tendency driven by the OHFC. In general, winter warming and sea ice retreat due to the OHFC forcing increase with time (i.e., the response is greater for the OHFC from years 470 to 500 following CO₂ doubling in the fully coupled models than for OHFC from earlier time periods; see Figure S8). In the NH, the Arctic Ocean (primarily the Nordic, Beaufort, and Chukchi Seas) warms and loses sea ice, while the surrounding land masses (boreal North America and NE Eurasia) warm (Figure 3e); in the SH, warming is limited to the margin of the Antarctic continent (primarily the Amundson-Bellinghousen Sea and the edge of the East Antarctic continental shelf region), with little warming over the Antarctic continent itself (Figure 3g). In both hemispheres, this winter polar warming is accompanied by subpolar cooling, notably over Greenland and the North Atlantic in the NH and ~60°S in the SH.

In summer, both hemispheres experience cooling with the imposed OHFC forcing (Figures 3f and 3h), though cooling is approximately 1 K greater in

the NH than the SH. This cooling, however, is accompanied by regions of modest summer warming that coincide with areas of winter season sea ice loss (compare summer sea ice fraction change contours in Figure 3h with Figure 3g and in Figure 3i with Figure 3j). Since summer temperatures are generally cooler, this decrease in summer sea ice must be a result of sea ice decline in the previous winter. Therefore, though OHU cools the high latitudes in summer, summer sea ice still declines because of increased winter season OHFC that thins and reduces the area of the ice pack.

3.3. Comparative Radiative Feedback Analysis

We assess the differing sensitivity of the Arctic and Antarctic by comparing their respective radiative feedback components (Figure 4). Feedback components in the first quadrant are destabilizing over both the Arctic and Antarctic in that they pull the global net TOA anomaly away from zero (i.e., away from radiative equilibrium); in contrast, feedback components in the third quadrant are stabilizing over both the Arctic and Antarctic in that they push the global net TOA anomaly back to zero (i.e., toward radiative equilibrium). Furthermore, feedbacks that lie to the right of the one-to-one line (all of which are in the first quadrant and are therefore

destabilizing over both poles) tend to pull the Arctic further away from TOA radiative equilibrium than those same feedbacks in the Antarctic. In contrast, the Planck feedback, which is stabilizing over both poles, lies to the left of the one-to-one line: it pulls the Arctic more strongly toward TOA radiative equilibrium than it does the Antarctic.

With CO₂ doubling only (i.e., without any oceanic changes), destabilizing radiative feedbacks (i.e., those that push the net TOA anomaly away from zero) are more destabilizing over the Arctic than the Antarctic (i.e., they lie to the right of the one-to-one line; Figure 4, large circle markers). In summer, this Arctic-Antarctic asymmetry is evident in the ice albedo, water vapor longwave (WV LW), water vapor shortwave (WV SW), and cloud feedbacks, all of which are more destabilizing over the Arctic than Antarctic (0.7, 0.6, 0.3, and 1.3 W/m²/K greater ice albedo; WV LW, WV SW, and cloud feedbacks in the Arctic relative to the Antarctic, respectively); in winter, this asymmetry is confined to the lapse rate feedback (1.4 W/m²/K greater in the Arctic than in the Antarctic). In contrast, the Planck feedback, which pulls the net TOA radiative anomaly back toward zero, compensates, albeit incompletely, by stabilizing the Arctic more than the Antarctic (i.e., the Planck feedback lies to the left of the one-to-one line and is 1.9 W/m²/K more stabilizing over the Arctic than the Antarctic; Figure 4).

When the various OHFC forcings are combined with CO₂ doubling, destabilizing feedbacks (i.e., those that pull the net TOA anomaly away from zero) respond more strongly over the Arctic than the Antarctic in all experiments. The most destabilizing feedbacks, the lapse rate feedback in winter, and the ice albedo feedback in summer, both become more destabilizing in the Arctic with the OHFC forcing (approximately 0.8 and 0.5 W/m²/K increase in the lapse rate and ice albedo feedbacks, respectively, over the Arctic in PertAtm+PertOcn165 relative to PertAtm); in the Antarctic, on the other hand, there is very little change in the magnitude of these feedbacks, except in the experiment utilizing OHFC forcing from years 470 to 500 (approximately 0.2 and 0.3 W/m²/K increase in the lapse rate and ice albedo feedbacks, respectively, over the Antarctic in PertAtm+PertOcn485 relative to PertAtm; Figure 4, small diamond markers). Though the winter season Planck feedback stabilizes radiative feedbacks over the Arctic, thereby counteracting some destabilization by the lapse rate feedback (Figure 4b, compare blue and purple markers), the OHFC forcings still destabilize the total temperature feedback (the sum of the Planck and lapse rate feedbacks; not shown) by approximately 0.3 W/m²/K over the Arctic compared to the Antarctic (in PertAtm+PertOcn75 relative to PertAtm). Incomplete compensation by the Planck feedback is also evident in the annual mean, where the more destabilizing ice albedo and lapse rate feedbacks over the Arctic with the added OHFC forcing are only partially offset by a more stabilizing Planck feedback (Figure 4c, compare blue and green markers with purple).

This ocean-forced amplification of destabilizing feedbacks is closely linked to the winter season poleward shift in the OHFC, which augments the lapse rate feedback by decreasing eddy-mediated moist static energy transport into the polar midtroposphere from the midlatitude surface (Feldl et al., 2017; Singh et al., 2017). The ice albedo feedback is also amplified because the winter season OHFC thins the sea ice and reduces its area, thereby priming the ice pack for greater summer season melt (Holland et al., 2010).

Feedback analysis shows that the ocean response to CO₂ doubling amplifies Arctic-Antarctic asymmetry by destabilizing temperature and ice albedo feedbacks more so over the Arctic than over the Antarctic. More stabilizing feedback processes over the Antarctic, and less sensitivity of these feedbacks to similar OHFC forcings may be explained (in part) by the smaller area over which these feedbacks operate over the Antarctic compared to the Arctic. Neither the ice albedo feedback nor the lapse rate feedback operate over the Antarctic continent itself (Figures S9 and S10); on the other hand, both lapse rate and ice albedo feedbacks are strongly destabilizing over both ocean and boreal land areas of the Arctic. When the perturbed OHFC is imposed, these destabilizing feedbacks are amplified over a greater area in the Arctic than the Antarctic, accounting for some of the greater sensitivity of the former.

4. Discussion

Forcings that are relatively symmetric between the hemispheres (either CO₂ doubling in isolation or hemispherically similar OHFC forcings, as in some GCMs such as the CESM) can give rise to hemispherically asymmetric climate responses. This result is evident from our analysis of GCMs participating in CMIP5 and is further corroborated from direct assessment of the equilibrium response to OHFC forcings and CO₂ doubling in the CESM-SOM. Overall, these results show that the Arctic and Antarctic regions have different intrinsic

sensitivities to forcings, whether the forcings are atmospheric (as for CO₂ doubling) or applied at the surface (as for changes in ocean heat convergence).

Our results show that the (transient) ocean response to CO₂ forcing magnifies asymmetries between the Arctic and Antarctic. However, the ocean does not merely curtail Antarctic warming by taking up more heat in the SH relative to the NH. We have shown that changes in ocean heat convergence destabilize radiative feedbacks over the Arctic, which amplifies Arctic climate sensitivity; the Antarctic, on the other hand, remains relatively impervious to the ocean response, except at very long time scales (i.e., the response to the OHFC forcing derived from years 470 to 500 in the fully coupled CO₂ doubling experiment). Destabilization of Arctic radiative feedbacks is closely tied to the poleward shift in the high-latitude OHFC, which amplifies the winter season lapse rate feedback (Singh et al., 2017); the increased summer season ice albedo feedback arises because of reduced summer sea ice amidst cooler summer season temperatures. Therefore, from a TOA perspective, the polar climate response to CO₂ forced OHFC anomalies is fundamentally a response to increased ocean heat transport into the high latitudes, not to subpolar heat uptake per se.

From a hemispheric perspective, the ocean response may actually decrease climate sensitivity asymmetry between the NH and SH in some models. While the ocean heat convergence cools both hemispheres in the annual mean, the feedbacks triggered by the ocean forcing (which are relatively symmetric in magnitude in the CESM) more efficiently dissipate the forcing in the SH than in the NH (i.e., λ_{eff} is more stabilizing in the SH than in the NH). Therefore, in models where differences in OHU between the hemispheres are small, the ocean response may actually cool the NH more than the SH and thereby decrease hemispheric asymmetries in climate sensitivity.

As shown in the idealized studies of Rose et al. (2014), the spatial pattern of OHU has a major impact on both the magnitude and spatial pattern of the climate system response. Our results support the finding that subpolar heat uptake is more efficacious than tropical heat uptake (compare the greater efficacy of the temperature response in CESM-SOM experiments using OHFC from years 150 to 180 after CO₂ doubling versus years 0–30 and 60–90). However, our results also show that the spatial pattern of OHU may impact its forcing efficacy in unexpected ways; subtle changes in the spatial pattern of OHU may result in very different hemispheric forcing efficacies (recall Figure 3e). Additionally, the sensitivity of Arctic and Antarctic climates to the ocean response strongly depends on the winter season poleward shift in the OHFC, which is not accounted for in such idealized experiments.

We conclude with some important caveats of the present study. First, we have analyzed the impact of the transient ocean response to CO₂ doubling in a single model; multimodel studies will have to be undertaken to confirm that the mechanisms described here can be generalized. Furthermore, we have not considered the role of Antarctic ozone depletion in our analysis, which may play a role in suppressed climate sensitivity over the Antarctic in the present day (see, e.g., Marshall et al., 2014). We have also assumed linearity in the forcing feedback framework, thereby neglecting the possibility that asymmetry between the climate system response to positive (e.g., CO₂) and negative (e.g., OHU) forcings may underpin differences in efficacy (see, e.g., Schaller et al., 2014, for a discussion in a solar geoengineering context). Finally, we have not considered how sensitivity may be impacted by multicentennial processes, including loss of the Greenland and Antarctic ice sheets; ice sheet orography, for example, may amplify sensitivity differences between the hemispheres (Salzmann, 2017). Indeed, ice sheet orography can be shown to damp the destabilizing high-latitude lapse rate feedback triggered by CO₂ forcings, a subject that we reserve for future study. Despite these caveats, our results suggest that at least some of the asymmetry between the Arctic and Antarctic may be ascribed to intrinsic differences in sensitivity and that the ocean response may further amplify these differences.

References

- Alexeev, V., Langen, P., & Bates, J. (2005). Polar amplification of surface warming on an aquaplanet in "ghost forcing" experiments without sea ice feedbacks. *Climate Dynamics*, 24, 655–666.
- Armour, K., Marshall, J., Scott, J., Donohoe, A., & Newsom, E. (2016). Southern Ocean warming delayed by circumpolar upwelling and equatorward transport. *Nature Geoscience*, 9, 549–554.
- Bailey, D., Hannay, C., Holland, M., & Neale, R. (2010). Slab ocean model forcing (Technical report). Boulder, CO: National Center for Atmospheric Research.
- Bintanja, R., van Oldenborgh, G., Drijfhout, S. S., Wouters, B., & Katsman, C. (2013). Important role for ocean warming and increased ice-shelf melt in Antarctic sea ice expansion. *Nature Geoscience*, 6, 376–379.
- Bitz, C., Gent, P., Woodgate, R., Holland, M., & Lindsay, R. (2006). The influence of sea ice on ocean heat uptake in response to increasing CO₂. *Journal of Climate*, 19, 2437–2450.

Acknowledgments

H. A. S. is grateful to the Linus Pauling Distinguished Postdoctoral Fellowship, sponsored by the U.S. DOE Office of Science's Pacific Northwest National Laboratory for facilities and funding. Support for O. A. G. and P. J. R. was provided by the Regional and Global Climate Modeling Program as a contribution to the HiLAT project. The Pacific Northwest National Laboratory is operated for the U.S. Department of Energy by Battelle Memorial Institute under contract DE-AC05-76RL01830. All authors acknowledge the World Climate Research Program's Working Group on Coupled Modeling, which is responsible for CMIP and thank the climate modeling groups (listed in the SI and Table 1) for producing and making available their model output. For CMIP, the U.S. DOE's Program for Climate Model Diagnosis and Intercomparison provides coordinating support and led development of software infrastructure in partnership with the Global Organization for Earth System Science Portals. Model output data generated for this study have been published on the Zenodo data repository at <https://doi.org/10.5281/zenodo.1283483>. Finally, all authors thank Greg Flato and two anonymous reviewers for helpful critiques of the submitted manuscript.

- Bitz, C., Holland, M., Hunke, E., & Moritz, R. (2005). Maintenance of the sea ice edge. *Journal of Climate*, *18*, 2903–2921.
- Bitz, C., Shell, K., Gent, P., Bailey, D., Danabasoglu, G., Armour, K., et al. (2012). Climate sensitivity in the Community Climate System Model, version 4. *Journal of Climate*, *25*(9), 3053–70.
- Comiso, J. (2002). A rapidly declining perennial sea ice cover in the Arctic. *Geophysical Research Letters*, *29*(20), 1956. <https://doi.org/10.1029/2002GL015650>
- Comiso, J. (2003). Warming trends in the Arctic from clear sky satellite observations. *Journal of Climate*, *16*, 3498–3510.
- Danabasoglu, G., Bates, S., Briegleb, B., Jayne, S., Jochum, M., Large, W., et al. (2012). The CCSM4 ocean component. *Journal of Climate*, *25*, 1361–1389.
- Feldl, N., Anderson, B., & Bordoni, S. (2017). Atmospheric eddies mediate lapse rate feedback and Arctic amplification. *Journal of Climate*, *30*, 9213–9224.
- Fetterer, F., Knowles, K., Meier, W., Savoie, M., & Windnagel, A. (2017). Sea ice index, version 3 (Tech. rep.) Boulder, CO: NSIDC: National Snow and Ice Data Center.
- Flato, G., & Boer, G. (2001). Warming asymmetry in climate change simulations. *Geophysical Research Letters*, *28*(1), 195–198.
- Garuba, O., Lu, J., Liu, F., & Singh, H. (2017). The active role of the ocean in the temporal evolution of climate sensitivity. *Geophysical Research Letters*, *45*, 306–315. <https://doi.org/10.1002/2017GL075633>
- Gettelman, A., Kay, J., & Holland, M. (2012). The evolution of climate sensitivity and climate feedbacks in the Community Atmosphere Model. *Journal of Climate*, *25*(5), 1453–1469.
- Hansen, J., Lacis, A., Rind, D., Russell, G., Stone, P., Fung, I., et al. (1984). Climate processes and climate sensitivity, geophysical monograph. Climate Sensitivity: Analysis of Feedback Mechanisms, American Geophysical Union.
- Holland, M., & Bitz, C. (2003). Polar amplification of climate change in coupled models. *Climate Dynamics*, *21*, 221–232.
- Holland, M., Serreze, M., & Stroeve, J. (2010). The sea ice mass budget of the Arctic and its future change as simulated by coupled climate models. *Climate Dynamics*, *34*, 185–200.
- Hunke, E., & Lipscomb, W. (2008). CICE: The Los Alamos Sea Ice Model, documentation and software, version 4.0 (Tech. Rep. LA-CC-06-012). New Mexico: Los Alamos National Laboratory.
- Hurrell, J., Holland, M., Gent, P., Ghan, S., Kay, J., Kushner, P., et al. (2013). The Community Earth System Model: A framework for collaborative research. *Bulletin of the American Meteorological Society*, *94*, 1339–1360.
- Hwang, Y.-T., & Frierson, D. (2010). Increasing atmospheric poleward energy transport with global warming. *Geophysical Research Letters*, *37*, L24807. <https://doi.org/10.1029/2010GL045440>
- Hwang, Y.-T., Frierson, D., & Kay, J. (2011). Coupling between Arctic feedbacks and changes in poleward energy transport. *Geophysical Research Letters*, *38*, L17704. <https://doi.org/10.1029/2011GL048546>
- Kay, J., Holland, M., Bitz, C., Blanchard-Wrigglesworth, E., Gettelman, A., Conley, A., & Bailey, D. (2012). The influence of local feedbacks and northward heat transport on the equilibrium Arctic climate response to increased greenhouse gas forcing. *Journal of Climate*, *25*, 5433–5450.
- Knutti, R., & Sedlacek, J. (2013). Robustness and uncertainties in the new CMIP5 climate model projections. *Nature Climate Change*, *3*, 369–373.
- Manabe, S., & Wetherald, R. (1975). The effects of doubling the CO₂ concentration on the climate of a General Circulation Model. *Journal of the Atmospheric Sciences*, *32*(1), 3–15.
- Marshall, J., Armour, K., Scott, J., Kostov, Y., Hausmann, U., Ferreira, D., et al. (2014). The ocean's role in polar climate change: Asymmetric Arctic and Antarctic responses to greenhouse gas and ozone forcing. *Philosophical Transactions of the Royal Society A*, *372*, 20130040.
- Neale, R., Chen, C.-C., Gettelman, A., Lauritzen, P., Park, S., Williamson, D., et al. (2012). Description of NCAR Community Atmosphere Model (CAM 5.0) (NCAR Technical Note TN-486+STR). Boulder, CO: NCAR.
- Oleson, K., Lawrence, D., Bonan, G., Flanner, M., Kluzek, E., Lawrence, P., et al. (2010). Technical description of version 4.0 of the Community Land Model (CLM) (Tech. Rep. TN-478+STR). Boulder, CO: National Center for Atmospheric Research.
- Pauling, A., Bitz, C., Smith, I., & Langhorne, P. (2016). The response of the Southern Ocean and Antarctic sea ice to freshwater from ice shelves in an Earth System Model. *Journal of Climate*, *29*, 1655–1672.
- Rose, B., Armour, K., Battisti, D., Feldl, N., & Koll, D. (2014). The dependence of transient climate sensitivity and radiative feedbacks on the spatial pattern of ocean heat uptake. *Geophysical Research Letters*, *41*, 1071–1078. <https://doi.org/10.1002/2013GL058955>
- Rose, B., & Rayborn, L. (2016). The effects of ocean heat uptake on transient climate sensitivity. *Current Climate Change Reports*, *2*(4), 190–201.
- Salzmann, M. (2017). The polar amplification asymmetry: Role of Antarctic surface height. *Earth System Dynamics*, *8*, 323–336.
- Schaller, N., Sedlacek, J., & Knutti, R. (2014). The asymmetry of the climate system's response to solar forcing changes and its implications for geoengineering scenarios. *Journal of Geophysical Research: Atmospheres*, *119*, 5171–5184. <https://doi.org/10.1002/2013JD021258>
- Shell, K., Kiehl, J., & Shields, C. (2008). Radiative kernel technique to calculate climate feedbacks in NCAR's Community Atmospheric Model. *Journal of Climate*, *21*, 2269–2283.
- Sigmond, M., & Fyfe, J. (2010). Has the ozone hole contributed to increased Antarctic sea ice extent? *Geophysical Research Letters*, *37*, L18502. <https://doi.org/10.1029/2010GL044301>
- Singh, H., Rasch, P., & Rose, B. (2017). Increased ocean heat transports into the high latitudes with CO₂ doubling enhance polar-amplified warming. *Geophysical Research Letters*, *44*, 10,583–10,591. <https://doi.org/10.1002/2017GL074561>
- Soden, B., Held, I., Colman, R., Shell, K., & Kiehl, J. (2008). Quantifying climate feedbacks using radiative kernels. *Journal of Climate*, *21*, 3504–3520.
- Steig, E., Schneider, D., Rutherford, S., Mann, M., Comiso, J., & Sindell, D. (2009). Warming of the Antarctic ice-sheet surface since the 1957 international geophysical year. *Nature*, *457*, 459–462.
- Stroeve, J., Holland, M., Meier, W., Scambos, T., & Serreze, M. (2007). Arctic sea ice decline: Faster than forecast. *Geophysical Research Letters*, *34*, L09501. <https://doi.org/10.1029/2007GL029703>
- Sutton, R., & Mathieu, P.-P. (2002). Response of the atmosphere-ocean mixed-layer system to anomalous ocean heat-flux convergence. *Quarterly Journal of the Royal Meteorological Society*, *128*, 1259–1275.
- Turner, J., Comiso, J., Marshall, G., Lachlan-Cope, T., Bracegirdle, T., Maksym, T., et al. (2009). Non-annular atmospheric circulation change induced by stratospheric ozone depletion and its role in the recent increase in Antarctic sea ice extent. *Geophysical Research Letters*, *36*, L08502. <https://doi.org/10.1029/2009GL037524>
- Turner, J., Overland, J., & Walsh, J. (2007). An Arctic and Antarctic perspective on recent climate change. *International Journal of Climatology*, *27*, 277–293.
- Walsh, J. (2009). A comparison of Arctic and Antarctic climate change. *Antarctic Science*, *21*(3), 179–188.